Corroborating ecological depth preferences of planktonic foraminifera in the tropical Atlantic with the stable oxygen isotope ratios of core top specimens

E. Christa Farmer,[1,2] Alexey Kaplan,[1] Peter B. de Menocal,[1] and Jean Lynch-Stieglitz[1,3]

Received 28 August 2006; revised 2 March 2007; accepted 11 April 2007; published 1 August 2007.

[1] Past variability in upper ocean thermocline depth is commonly estimated from the abundance of different species of planktonic organisms or the difference in oxygen isotopic composition between two species of planktonic foraminifera, one that lives in the mixed layer and one that lives in or near the thermocline. To test the latter relationships, we measured the oxygen isotopic composition of eight species of planktonic foraminifera (pink and white varieties of *Globigerinoides ruber*, *Globigerinoides sacculifer* without the final chamber, *Orbulina universa*, *Pulleniatina obliquiloculata*, *Globorotalia menardii*, *Neogloborotalia dutertrei*, and *Globorotalia tumida*) in surface sediment samples from 31 tropical Atlantic deep-sea sediment cores. Bayesian analysis was used to compare measured oxygen isotopic compositions with their predictions based on modern data sets of annual temperatures and oxygen isotopic composition of ocean water in the upper 500 m at the core sites. Posterior probability densities for predictive model parameters were computed. Probability distributions of calcification depth for analyzed species corroborated their ecological preferences inferred from net tow and sediment trap data. Robustness of the habitat signals in core top specimens suggests that reconstructions of the entire upper ocean temperature profiles, not just their thermocline depth or temperature, might be possible.

Citation: Farmer, E. C., A. Kaplan, P. B. de Menocal, and J. Lynch-Stieglitz (2007), Corroborating ecological depth preferences of planktonic foraminifera in the tropical Atlantic with the stable oxygen isotope ratios of core top specimens, *Paleoceanography*, *22*, PA3205, doi:10.1029/2006PA001361.

1. Introduction

[2] Study of the variation in water column depth preference among various species of planktonic foraminifera was pioneered by *Bé and Tolderlund* [1971] and furthered by *Fairbanks and Wiebe* [1980] using Multiple Opening/Closing Net and Environmental Sampling System tows in the western North Atlantic. *Globigerinoides ruber* (both pink and white varieties) and *Globigerinoides sacculifer* (without final chamber) species were most common in the surface mixed layer, whereas *Globorotalia menardii* and *Neogloborotalia dutertrei* were most abundant at the thermocline. *Orbulina universa* was often most abundant in the mixed layer but also sometimes most abundant in the thermocline (hence its "universal" name). Below the photic zone, at depths down to several hundred meters, the most abundant species were *Globorotalia truncatulinoides*, *Globorotalia crassiformis*, and *Globorotalia tumida*. Oxygen isotope ratios ($\delta^{18}O$) predicted from hydrography at the depth at which each species was found living matched well with isotopic values measured in core top samples of each species [*Fairbanks and Wiebe*, 1980; *Ravelo and Fairbanks*, 1992].

[3] *Deuser and Ross* [1989] collected planktonic foraminiferal samples from sediment traps in the Sargasso Sea and compared their $\delta^{18}O$ with hydrography as well. They estimated that *G. ruber* (pink variant) represented conditions in the surface waters and that *Pulleniatina obliquiloculata*, *Globorotalia inflata*, and *N. dutertrei* represented conditions in the winter mixed layer (down to 100 m water depth), while *Globigerinoides conglobatus* represented the depth interval of 75–100 m during the fall season. *Mulitza et al.* [1997] proposed that past changes in upper ocean thermal stratification could be estimated on the basis of the calculated $\delta^{18}O$ gradient between surface-dwelling species (*G. sacculifer* and *Neogloboquadrina pachyderma*, right-coiling variant) and deeper dwelling *G. truncatulinoides* which appeared to calcify near 250 m. On the basis of these results and some further data for *G. ruber* (pink variant), *Mulitza et al.* [1998] proposed a theoretical model by which the temperature at various water depths can be "triangulated" from at least three species of planktonic foraminifera.

[4] *Dekens et al.* [2002] looked at both calcite $\delta^{18}O$ (hereinafter $\delta^{18}O_c$) and Mg/Ca values from core top sediment samples in the tropics of all oceans, confirming that

[1]Lamont-Doherty Earth Observatory of Columbia University, Palisades, New York, USA.
[2]Now at Geology Department, Hofstra University, Hempstead, New York, USA.
[3]Now at School of Earth and Atmospheric Sciences, Georgia Institute of Technology, Atlanta, Georgia, USA.

0883-8305/07/2006PA001361$12.00

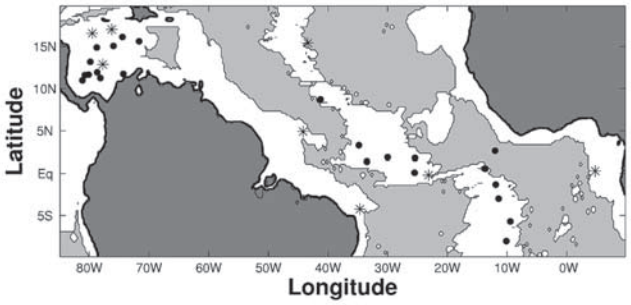

Figure 1. Map showing location of all cores (all depths below 4150 m isobath are shaded gray). Dots show locations of 23 cores for which oxygen isotope data were obtained for all eight species used in the analysis; stars show the locations of eight cores for which data were obtained for only some of the species. Note that though VM019-297 at 2.617°N, 12.000°W appears below the 4150 m isobath, it is located on a local high point at 4122 m (see Table 1).

G. ruber record surface temperatures, *G. sacculifer* record temperatures at 20–30 m, and the depth habitat of *N. dutertrei* is more broad but seems to be about 50 m. *Anand et al.* [2003] also measured both $\delta^{18}O_c$ and Mg/Ca from sediment trap samples, reaching similar conclusions. *LeGrande et al.* [2004] took a slightly different approach, measuring $\delta^{18}O_c$ of *Globorotalia truncatulinoides* and comparing it to upper ocean water $\delta^{18}O$ (hereinafter $\delta^{18}O_w$) and temperature. The best match indicated that the species either calcified at 350 m or calcified at the surface and added postgametogenic calcite at 800 m. *Schmidt and Mulitza* [2002] used a Monte Carlo minimization procedure to match foraminiferal $\delta^{18}O_c$ for six mixed layer species from a global data set of core tops with data sets of $\delta^{18}O_w$ and temperatures. They produced a description of temperature ranges and other ecological conditions preferred by these species.

[5] Here we investigate whether the tropical Atlantic habitat depth preferences of eight species of planktonic foraminifera are consistent with the $\delta^{18}O_c$ of core top specimens. Using a Bayesian analysis approach, measurements of $\delta^{18}O_c$ in these species are compared with expected values on the basis of published calibration equations and analyzed data sets of ocean water temperatures [*Conkright et al.*, 2002] (available at http://iridl.ldeo.columbia.edu/SOURCES/.NOAA/.NODC/.WOA01/ accessed 2004) and $\delta^{18}O_w$ [*LeGrande and Schmidt*, 2006]. Our newly produced $\delta^{18}O_c$ data set is smaller in size but also smaller in the geographical extent than the data set used by *Schmidt and Mulitza* [2002]. Consequently, we can use calcification depth as a main factor defining the habitat of a given species and allow, within some limits, species-dependent coefficients in their $\delta^{18}O_c$-to-temperature relationship.

2. Methods

2.1. Study Area

[6] In order to test the relationship between ocean water properties and the isotopic oxygen composition of multiple species of calciferous planktonic foraminifera this study uses modern seafloor sediment samples from the tropical Atlantic. The oxygen isotope ratio of foraminiferal calcite, $\delta^{18}O_c$, is a function of temperature and the oxygen isotope ratio of seawater, $\delta^{18}O_w$ [*Berger*, 1981; *Craig and Gordon*, 1965]. Tropical Atlantic surface salinity variations have little effect on $\delta^{18}O_c$ of foraminifera formed in the mixed layer because rainfall $\delta^{18}O$ is very close to that of the seawater. Changes in the water balance that affect salinity do not change the $\delta^{18}O_w$ of surface waters as much as they do in other parts of the Atlantic Ocean or in other ocean basins [*Schmidt*, 1999; *LeGrande and Schmidt*, 2006; G. A. Schmidt et al., Global seawater oxygen-18 database, 1999, available at http://data.giss.nasa.gov/o18data/]. Deeper waters, however, reflect the salinity and $\delta^{18}O_w$ of higher latitudes [*Sarmiento et al.*, 2004]; hence these parameters influence the $\delta^{18}O_c$ of foraminifera calcifying below the mixed layer.

[7] Samples were collected from the top centimeter of 31 cores in a transect from the Caribbean to the Gulf of Guinea (Figure 1 and Table 1). The cores were selected from the Lamont-Doherty Earth Observatory Deep-Sea Sample Repository on the basis of their full representation of the thermocline depth gradient in the tropical Atlantic (Figure 2a). Sediments from the tops of these cores are expected to be of modern or of late Holocene age based on stratigraphic information, like the presence or absence of faunal markers. Additionally, only cores collected at water depths of less than 4150 m were included (see Table 1) in order to avoid the influence of $CaCO_3$ dissolution below the tropical Atlantic lysocline [*Broecker and Takahashi*, 1978; *Lohmann*, 1995].

2.2. Sample Preparation

[8] Sediment samples were shaken in a sodium metaphosphate surfactant solution for about 2 hours, washed through 150 μm sieves with deionized water, and dried in a 50°C oven. The fine (<150 μm) fraction was archived, and the coarse fraction was sieved in narrow size fractions to minimize the known ontogenetic fractionation effects of foraminiferal growth and size. The size ranges differed between species but were selected to balance between the ideal size range where the growth effect is minimal and the size range in which the species is abundant (see Table 2). Between 10 and 20 individuals per species were picked from each sample with a red sable brush. The $\delta^{18}O_c$ of all foraminiferal species from each core was measured using a Micromass Optima mass spectrometer with a Multiprep individual acid bath carbonate preparation device. Measurement precision is estimated from the 1-σ reproducibility of multiple measurements of a known standard in each run, averaged over all runs: 0.02‰ for $\delta^{13}C$ and 0.06‰ for $\delta^{18}O$.

2.3. Instrumental Data and Calibration Relationships

[9] Foraminiferal calcite oxygen isotope ratios ($\delta^{18}O_c$) for each species from all cores were compared to the values predicted on the basis of existing analyses of mean water temperature and $\delta^{18}O_w$. Temperature data were taken from the 2001 NOAA World Ocean Atlas (WOA2001) [*Conkright et al.*, 2002] (accessed 2004). Mean temperatures, objectively

Table 1. Data Produced in This Analysis[a]

				$\delta^{18}O_c$, ‰							
Core ID	Latitude, deg	Longitude, deg	Water Depth, km	WRU	PRU	SAC	UNI	OBL	MEN	DUT	TUM
VM028-126[b]	10.983	−81.150	3.162	−1.60	−1.94	−1.17	−0.93	−0.71	−0.26	−0.53	−0.06
VM028-128[b]	11.600	−80.750	3.264	−1.66	−1.72	−1.20	−1.13	−0.68	−0.48	−0.56	0.34
VM028-127[b]	11.650	−80.133	3.237	−1.76	−1.62	−1.34	−1.04	−0.58	−0.27	−0.48	−0.02
RC013-158[b]	13.183	−79.833	3.016	−1.73	−1.74	−1.39	−0.89	−0.64	−0.46	−0.68	−0.05
RC010-049	16.567	−79.517	1.238	−2.11		−1.61					−0.29
RC013-154[b]	14.883	−78.750	2.308	−1.90	−1.96	−1.61	−1.45	−1.13	−0.74	−1.07	−0.71
VM028-122[b]	11.933	−78.683	3.623	−1.49	−1.58	−1.42	−0.47	−0.45	−0.13	−0.30	0.41
RC013-157[b]	11.250	−78.150	3.588	−1.44	−1.72	−1.23	−0.98	−0.54	0.00	−0.31	0.64
RC013-155	12.867	−77.750	3.930	−1.92	−1.89	−1.43	−0.32		−0.50	−0.52	0.32
VM026-125	17.033	−76.233	2.210	−2.21	−2.18	−1.97			−0.87		−0.45
RC013-153[b]	15.067	−75.950	1.777	−1.55	−2.14	−1.43	−0.96	−0.71	−0.74	−0.57	0.21
VM026-124[b]	16.133	−74.450	3.005	−1.98	−1.94	−1.51	−1.06	−1.13	−0.71	−0.72	−0.45
RC013-148[b]	11.745	−74.288	1.257	−1.51	−1.55	−1.31	−0.15	−0.60	−0.38	−0.48	0.30
RC013-150[b]	15.617	−71.667	3.788	−2.13	−2.12	−1.67	−0.37	−1.14	−0.80	−0.61	0.07
VM018-022	4.900	−44.167	4.145	−1.63	−1.55	−1.37	−1.44	−0.79	−0.74		0.48
VM016-205	15.400	−43.400	4.043	−1.03	−1.32	−0.80	−0.94		−0.85	0.26	0.26
VM022-026[b]	8.717	−41.250	3.720	−1.58	−1.75	−1.19	−1.77	−0.79	−0.01	−0.25	0.63
VM025-060[b]	3.283	−34.833	3.749	−1.67	−1.57	−1.27	−1.39	−0.87	−0.64	0.18	0.11
VM020-227	−4.233	−34.633	3.812	−1.01		−1.58			−0.63		−0.04
VM025-059[b]	1.367	−33.483	3.824	−1.89	−1.82	−1.58	−1.61	−0.99	−0.24	−0.11	−0.04
RC013-189[b]	1.867	−30.000	3.233	−1.70	−1.71	−1.56	−1.74	−1.06	−0.43	−0.98	0.27
VM027-181[b]	0.067	−25.500	3.601	−1.58	−1.47	−1.37	−1.30	−0.69	−0.36	−0.54	0.52
RC013-190[b]	1.783	−25.433	3.797	−1.19	−1.42	−1.09	−0.95	−0.62	−0.53	−0.04	0.59
VM030-040	−0.200	−23.150	3.706	−1.51	−1.23	−1.17	−1.29		−0.39	−0.43	0.42
RC024-001[b]	0.550	−13.650	3.837	−1.59	−1.53	−1.17	−0.98	−0.64	−0.27	−0.20	0.79
VM019-297[b]	2.617	−12.000	4.122	−1.36	−1.54	−1.13	−0.25	−0.58	0.37	−0.12	0.57
RC024-007[b]	−1.330	−11.900	3.899	−1.21	−1.77	−1.03	−1.41	−0.63	−0.31	−0.43	0.65
RC024-012[b]	−3.000	−11.417	3.486	−1.62	−1.63	−1.00	−0.76	−0.48	0.31	−0.56	0.87
RC024-022[b]	−8.033	−10.133	3.882	−1.23	−1.82	−1.10	−0.85	−0.73	−0.30	−0.11	0.34
RC024-018[b]	−5.700	−9.450	3.400	−1.63	−1.75	−1.21	−1.37	−0.97	−0.34	−0.56	0.28
VM019-284	0.267	4.767	3.937	−1.84		−1.09			0.25		1.10
N_{cores}				31	28	31	27	24	30	26	31

[a]Core locations are arranged from west to east. Measured $\delta^{18}O_c$ is given for eight species of planktonic foraminifera: WRU, *G. ruber* (white); PRU, *G. ruber* (pink); SAC, *G. sacculifer* (without final chamber); UNI, *O. universa*; OBL, *P. obliquiloculata*; MEN, *G. menardii*; DUT, *N. dutertrei*; and TUM, *N. tumida*. N_{cores} is number of cores in which each species was measured.
[b]All eight species were measured for core.

analyzed, were used in the 14 top water depth intervals: 0, 10, 20, 30, 50, 75, 100, 125, 150, 200, 250, 300, 400, and 500 m below the sea surface. Temperature values were interpolated bilinearly from a 1° × 1° WOA2001 spatial grid to the core locations. Mean seawater oxygen isotope ratios ($\delta^{18}O_w$) were taken from a recently produced three-dimensional (3-D) gridded data set by *LeGrande and Schmidt* [2006] (available at http://data.giss.nasa.gov/o18data/grid.html). Since the grids of this data set match those of WOA2001, our processing of $\delta^{18}O_w$ data was identical to the processing of water temperature profiles. Vertical profiles of water temperatures and $\delta^{18}O_w$ at core locations are shown in Figure 2.

[10] To date, most foraminifera species used in our analysis do not have calibrations developed specifically for them. Therefore we inform our interpretation of $\delta^{18}O_c$ measurements by commonly used calibration equations for the planktonic foraminifera: those developed by *Bemis et al.* [1998] for the culture experiments with *O. universa* and *G. sacculifer* and those reported by *Mulitza et al.* [2003] based on samples of living *G. ruber* and *G. sacculifer* pumped from surface waters of the Atlantic. These calibrations all express water temperature *T* via a difference in

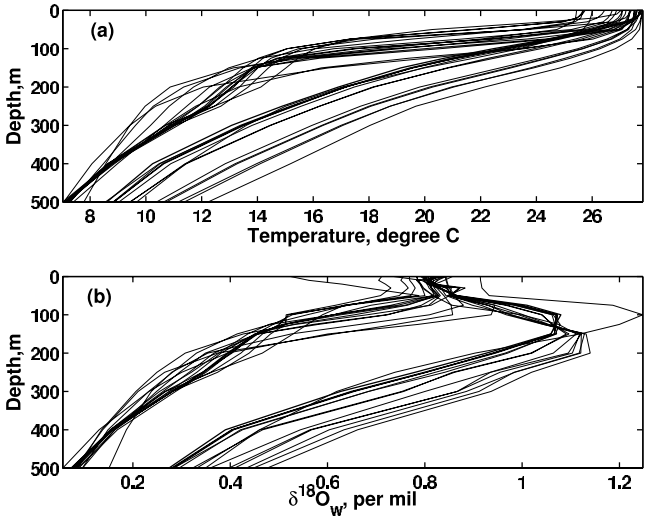

Figure 2. Mean annual ocean water (a) temperatures from *Conkright et al.* [2002] (available at http://iridl.ldeo.columbia.edu/SOURCES/.NOAA/.NODC/.WOA01/ accessed 2004) and (b) stable oxygen isotope ratios $\delta^{18}O_w$ from the analysis of *LeGrande and Schmidt* [2006] at all 31 core locations used in this study.

Table 2. Species and Size Fractions of Planktonic Foraminifera Used in This Analysis With References Used to Determine Size Fraction for Each Species

Species	Size Fraction		Source
	Minimum	Maximum	
G. ruber (white)	355	425	S. Mulitza (personal communication, 1998)
G. ruber (pink)	355	425	S. Mulitza (personal communication, 1998)
G. sacculifer	355	425	S. Mulitza (personal communication, 1998)
O. universa	500	600	*Ravelo and Fairbanks* [1992]
P. obliquiloculata	500	600	*Ravelo and Fairbanks* [1992]
G. menardii	600	710	*Ravelo and Fairbanks* [1992]
N. dutertrei	500	600	*Ravelo and Fairbanks* [1992]
N. tumida	500	600	*Ravelo and Fairbanks* [1992]

oxygen isotope ratios between calcite and water, $\delta^{18}O_c - \delta^{18}O_w$: The relationship

$$T = 14.9 - 4.8\left(\delta^{18}O_c - \delta^{18}O_w\right) \quad (1)$$

was obtained from culture experiments with *O. universa* under high-light conditions [*Bemis et al.*, 1998];

$$T = 16.5 - 4.8\left(\delta^{18}O_c - \delta^{18}O_w\right) \quad (2)$$

was obtained from culture experiments with *O. universa* under low-light conditions [*Bemis et al.*, 1998];

$$T = 14.2 - 4.44\left(\delta^{18}O_c - \delta^{18}O_w\right) \quad (3)$$

was obtained from *G. ruber* specimens pumped from the surface ocean [*Mulitza et al.*, 2003];

$$T = 14.91 - 4.35\left(\delta^{18}O_c - \delta^{18}O_w\right) \quad (4)$$

was obtained from *G. sacculifer* specimens pumped from the surface ocean [*Mulitza et al.*, 2003];

$$T = 13.2 - 4.89\left(\delta^{18}O_c - \delta^{18}O_w\right) \quad (5)$$

was obtained from culture experiments with *Globigerina bulloides* (12 chambered) [*Bemis et al.*, 1998].

2.4. Statistical Analysis

[11] Our goal is to analyze the measured values of $\delta^{18}O_c$ in order to determine the likely depths in the upper water column at which each species of foraminifera was calcifying. Calibrations (1)–(5) specify the relationship between temperature T and oxygen isotope ratios $\delta^{18}O_c$ and $\delta^{18}O_w$ in the form

$$T = \alpha - \beta\left(\delta^{18}O_c - \delta^{18}O_w\right)$$

for certain values of α and β. Temperatures T and seawater oxygen isotope ratios $\delta^{18}O_w$ in this relationship should be taken at some species-specific calcification depth z to be determined. The importance of species-specific calibration equations for temperature reconstruction efforts having been demonstrated [*Bemis et al.*, 2002], we allow coefficients α and β to be different for different species. Therefore we assume that the relationship

$$T(z) = \alpha - \beta\left[\delta^{18}O_c - \delta^{18}O_w(z)\right] \quad (6)$$

holds, within some error bounds, for each species for certain species-dependent values of α, β, and z. With an additional assumption that mean vertical profiles of T and $\delta^{18}O_w$ given by the present-time hydrographic data sets by *Conkright et al.* [2002] (accessed 2004) and *LeGrande and Schmidt* [2006], respectively, are applicable to the period when the foraminifera from the analyzed core tops were calcifying, we consider $T(z)$ and $\delta^{18}O_w(z)$ at all core locations to be known functions of z. With $\delta^{18}O_c$ measured, we can put the problem of estimating z, α, and β into the Bayesian framework [*Gelman et al.*, 2004].

[12] If values of α and β were known, as well as the calcification depth z, we could invert (6) to predict the measured values of $\delta^{18}O_c$ as

$$\delta^{18}O_c \approx \frac{\alpha}{\beta} - \frac{1}{\beta}T(z) + \delta^{18}O_w(z). \quad (7)$$

This model is approximate because there are measurement errors, errors associated with a calibration relationship, and errors due to the difference between the actual values of $T(z)$ and $\delta^{18}O_w(z)$ during calcification and their values that were obtained from the modern data sets, as well as the error in the paradigm that foraminifera calcified at a single depth. Assuming the total error in the relationship (7) to be normally distributed with zero mean and variance σ^2, we can write down the sampling distribution, i.e., the distribution of a measured value $\delta^{18}O_c$ conditional on all other parameters, as

$$\delta^{18}O_c|\alpha,\beta,z,\sigma^2 \sim N\left(\frac{\alpha}{\beta} - \frac{1}{\beta}T(z) + \delta^{18}O_w(z), \sigma^2\right)$$

or, in terms of its probability density function (pdf),

$$p\left(\delta^{18}O_c|\alpha,\beta,z,\sigma^2\right) = \frac{1}{\sqrt{2\pi}\sigma}\exp\left\{-\frac{1}{2\sigma^2}\left[\delta^{18}O_c - \delta^{18}O_w(z) + \frac{1}{\beta}T(z) - \frac{\alpha}{\beta}\right]^2\right\}.$$

For measurements $\{\delta^{18}O_c\} = \{\delta^{18}O_{c1}, \delta^{18}O_{c2}, \cdots, \delta^{18}O_{cN}\}$ made on N cores, the joint sampling distribution will be the product of individual ones:

$$p\left(\left\{\delta^{18}O_c\right\}|\alpha,\beta,z,\sigma^2\right) = \frac{1}{(2\pi)^{N/2}\sigma^N}\exp\left(-\frac{1}{2\sigma^2}\sum_{i=1}^{N}Y_i^2\right), \quad (8)$$

where

$$Y_i = \delta^{18}O_{ci} - \delta^{18}O_{wi}(z) + \frac{1}{\beta}T_i(z) - \frac{\alpha}{\beta}, \quad i = 1, \cdots, N \quad (9)$$

are differences between measured and predicted values of $\delta^{18}O_c$ for individual cores.

[13] Bayesian data analysis utilizes measurements by inverting predictive distribution (8) to obtain a "posterior" distribution for model parameters (that is, their conditional distribution, given all measured values):

$$p(\alpha, \beta, z, \sigma^2 | \{\delta^{18}O_c\}) = \frac{p(\{\delta^{18}O_c\} | \alpha, \beta, z, \sigma^2) p(\alpha, \beta, z, \sigma^2)}{p(\{\delta^{18}O_c\})}. \quad (10)$$

Here $p(\alpha, \beta, z, \sigma^2)$ is a "prior" distribution of these parameters (that is, our assumption about them was made before any measurements became available). Further,

$$p(\{\delta^{18}O_c\}) = \iiiint p(\{\delta^{18}O_c\} | \alpha, \beta, z, \sigma^2) \cdot p(\alpha, \beta, z, \sigma^2) d\alpha d\beta dz d\sigma^2$$

is just a normalizing factor, ensuring that $p(\alpha, \beta, z, \sigma^2 | \{\delta^{18}O_c\})$ defined by (10) integrates to 1 over its joint domain of α, β, z, and σ^2.

[14] Before any information about measurements of $\delta^{18}O_c$ is given, we can expect α and β to take with equal probability any values in their range known from published calibrations. We take these ranges of applicable values from equations (1)–(5) and then extend them by approximately two typical standard deviations of error in the published estimates of α and β, i.e., 0.3°C and 0.2°C/‰, respectively [*Bemis et al.*, 1998]. Therefore we take prior probability distributions for α and β to be uniform in the following ranges:

$$\alpha \sim U(12.5°C, 17°C), \quad \beta \sim U(3.9°C/‰, 5.3°C/‰).$$

Similarly, a natural choice of the prior distribution for z is a uniform distribution on an interval which is wide enough to contain the actual calcification depths of species that we analyze. Since net tow data indicated that all species analyzed here live within the interval between surface and 500 m, we use as a prior distribution

$$z \sim U(0 \text{ m}, 500 \text{ m}).$$

A standard approach to selecting a noninformative prior distribution for a variance parameter like σ^2 is to use a uniform distribution for its logarithm rather than the parameter itself [*Gelman et al.*, 2004]. The interval between 0.05 and 1‰ is wide enough to contain the standard deviation of the expected error in any useful prediction, thus we use a prior distribution $U(\ln 0.05, \ln 1)$ for $\ln \sigma$. Therefore

$$p(\alpha, \beta, z, \sigma^2) = U(12.5°C, 17°C) U(3.9°C/‰, 5.3°C/‰) \cdot U(z | 0 \text{ m}, 500 \text{ m}) U(\ln \sigma | \ln 0.05, \ln 1)/2\sigma^2. \quad (11)$$

(Note that variable changes in probability density functions between σ^2, σ, and $\ln\sigma$ are made according to the rules $p(\cdots, \sigma^2) = p(\cdots, \ln \sigma)/2\sigma^2$, $p(\cdots, \sigma) = p(\cdots, \ln \sigma)/\sigma$).

[15] Combining formulas (8), (10), and (11), we obtain

$$p(\alpha, \beta, z, \sigma^2 | \{\delta^{18}O_c\}) = C \begin{cases} \exp\left(-\frac{1}{2\sigma^2}\sum_{i=1}^N Y_i^2\right)/\sigma^{N+2}, & \text{if } 12.5 < \alpha < 17, \\ & 3.9 < \beta < 5.3, \\ & 0 < z < 500, \\ & 0.05 < \sigma < 1, \\ 0, & \text{otherwise}, \end{cases} \quad (12)$$

where Y_i are defined by (9) and a normalizing factor C is determined by the condition

$$\iiiint p(\alpha, \beta, z, \sigma^2 | \{\delta^{18}O_c\}) d\alpha d\beta dz d\sigma^2 = 1. \quad (13)$$

[16] The calculations were performed in Matlab. Values of the function

$$\exp\left(-\frac{1}{2\sigma^2}\sum_{i=1}^N Y_i^2\right)/\sigma^{N+2}$$

were tabulated on a grid covering the 4-D domain of α, β, z, and $\ln \sigma$ in which the probability density $p(\alpha, \beta, z, \sigma^2 | \delta^{18}O_{c1}, \delta^{18}O_{c2}, \cdots, \delta^{18}O_{cN})$ is nonzero, as defined by (12). Uniform grids of 40 points were used for α, β, and $\ln \sigma$, and the 14 grid points from WOA2001 were used for z. Normalizing factor C was computed from (13) using numerical integration; thus the full joint posterior probability density function (12) for all parameters became available. Marginal distributions were computed by further numerical integration:

$$\begin{aligned} p(\alpha, \beta, z) &= \int p(\alpha, \beta, z, \sigma^2 | \{\delta^{18}O_c\}) d\sigma^2, \\ p(\alpha, \beta) &= \iint p(\alpha, \beta, z, \sigma^2 | \{\delta^{18}O_c\}) dz d\sigma^2, \\ p(\alpha) &= \int p(\alpha, \beta) d\beta, \qquad p(\beta) = \int p(\alpha, \beta) d\alpha, \\ p(z) &= \iiint p(\alpha, \beta, z, \sigma^2 | \{\delta^{18}O_c\}) d\alpha d\beta d\sigma^2, \\ p(\sigma) &= 2\sigma \iiint p(\alpha, \beta, z, \sigma^2 | \{\delta^{18}O_c\}) d\alpha d\beta dz. \end{aligned} \quad (14)$$

These distributions for parameter values were then used to compute their means and confidence intervals.

[17] Prediction of the values that depend on the estimated parameters is done by the integration over the entire parameter space; that is, we compute

$$\langle \delta^{18}O_c \rangle = \iiint \left[\frac{\alpha}{\beta} - \frac{1}{\beta} T(z) + \delta^{18}O_w(z) \right] p(\alpha, \beta, z) d\alpha d\beta dz, \tag{15}$$

$$\langle T \rangle = \iiint \{ \alpha - \beta [\delta^{18}O_c - \delta^{18}O_w(z)] \} p(\alpha, \beta, z) d\alpha d\beta dz \tag{16}$$

for predictions of $\delta^{18}O_c$ and ocean temperature at the calcification depth. Uncertainties in these predictions are computed using these integrals and similar ones but with the predictive function squared:

$$\sigma_T^2 = \langle T^2 \rangle - \langle T \rangle^2$$

for the standard deviation σ_T of error in predictions of T, etc.

3. Results

[18] Eight planktonic foraminifer species were found in more than 20 cores and thus were sufficiently abundant for the statistical analysis. These were *G. ruber* (both pink and white variants) and *G. sacculifer* (without a final sac-like chamber) from the 355–425 μm size fraction; *O. universa*, *P. obliquiloculata*, and *G. menardii* from the 600–710 μm size fraction; and *N. dutertrei* and *G. tumida* from the 500–600 μm size fraction. Data are presented in Table 1, and size fractions are listed in Table 2.

3.1. Parameter Estimates

[19] The analysis method described in section 2 was applied to all measurements presented in Table 1 to each species separately. Figure 3 illustrates the analysis results for *G. ruber* (white) by presenting marginal posterior probability density functions of all parameters, computed by equation set (14). For easier interpretation, isolines of joint pdfs for (α, β) pairs (Figure 3a) are labeled not by the probability density value but by the probability with which this value is exceeded. For example, the contour marked "95%" surrounds the area of (α, β) values with cumulative probability of 0.95. Areas of high probability reach limits of the ranges set by prior distributions for both α and β values, suggesting that these parameters are not well constrained by the data in this analysis. Indeed, the individual marginal pdf for β (Figure 3b) reaches its maximum at the high limit of the range set by the prior distribution and remains high in most of the range. The marginal pdf for α (Figure 3c) shows that it is only slightly better constrained than β. However, pdfs for the calcification depth z and calibration error σ (Figures 3d and 3e) have large probability density values concentrated on relatively small segments of the prior range; hence these parameters are well constrained.

[20] The tendency of z and σ to be better constrained than α and β parameters holds for all species. This can be concluded from inspection of Table 3, which provides expected values (means of posterior distributions) and 95% confidence intervals of parameters for analyses of all species. This outcome is particularly important for our analysis of the calcification depth of different species. Figure 4 puts together their posterior pdfs for z, creating a striking pattern of species' inferred distribution in the water column which is quite consistent with their known ecological preferences.

[21] *Fairbanks and Wiebe* [1980] and *Dekens et al.* [2002] reported that *G. ruber* (both pink and white variants) and *G. sacculifer* (without final chamber) were most common in the mixed layer. Consistent with these results, our analysis suggests that *G. ruber* calcified in the top 30 and 40 m for white and pink variants, respectively, their expected depths being 16 and 21 m. The expected calcification depth of *G. sacculifer* (without final chamber), from our analysis, is near 30 m, with a rather narrow 95% confidence interval between 18 and 40 m.

[22] Our results for *O. universa* are also consistent with the *Fairbanks and Wiebe* [1980] data: The 95% confidence interval, covering the top 60 m encompasses therefore both the mixed layer and upper thermocline. *Ravelo and Fairbanks* [1992] found that *P. obliquiloculata* was most abundant at 60 m, near the base of the seasonal thermocline: This agrees well with our estimate of 50 m for its calcification depth. Our results also include an expected calcification depth near 100 m for *N. dutertrei* (albeit, with a wide confidence interval of 64–169 m) and near 75 m for *G. menardii* (with a narrow confidence interval between 63 and 87 m): Both these depths are consistent with the conclusions of *Fairbanks and Wiebe* [1980] and *Dekens et al.* [2002]. The depth range of 176–273 m obtained in our analysis for *G. tumida*, suggesting that this species calcifies below the thermocline, also matches well with the *Fairbanks and Wiebe* [1980] net tow results.

3.2. Model Consistency Checks

[23] As a summary measure of the model fit we perform the omnibus χ^2 discrepancy test [*Gelman et al.*, 2004, section 6.5, equation (6.4)], which in our case amounts to the statistic

$$\chi^2 = \sum_{i=1}^{i=N} Y_i^2 / \sigma^2, \tag{17}$$

where Y_i are model discrepancies computed by (9) for observed values of $\delta^{18}O_{ci}$ and a certain set of model parameters. In general, statistic (17) is a function of the parameters α, β, z, and σ. We take these parameters at their posterior means and report sample values of (17) in Table 4. Under a null hypothesis that model errors are normal with zero mean distribution, these sample values can be interpreted as coming from the χ^2 distribution with $N - 4$ degrees of freedom (four parameters were selected on the basis of N data points). Corresponding p values of the two-sided test to the null hypothesis, i.e., the theoretical probability that the χ^2-distributed random variable with $N - 4$ degrees of freedom would reach further toward the

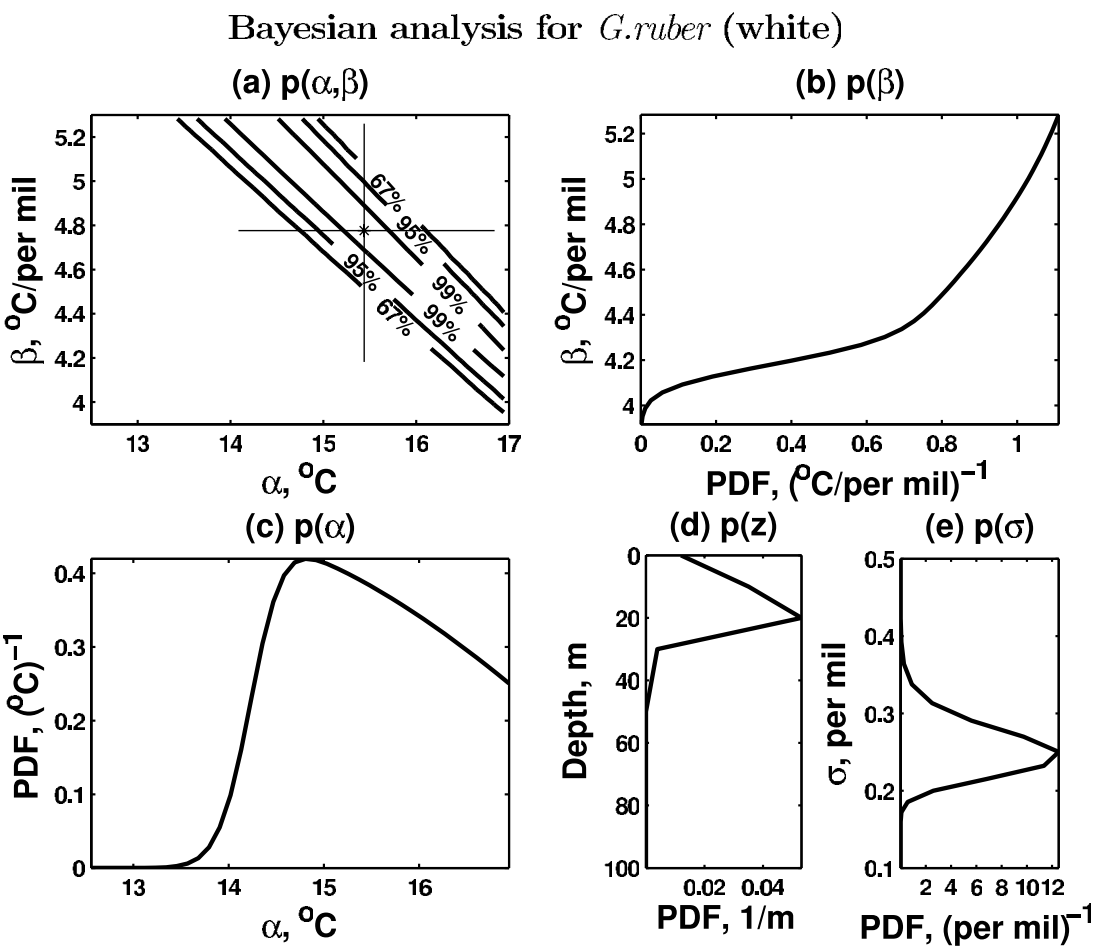

Figure 3. Results of Bayesian analysis for *G. ruber* (white). (a) Joint posterior probability density function (pdf) for calibration coefficients α and β (the star indicates the mean of the posterior distribution, with thin lines showing 95% confidence intervals for individual marginal distributions of α and β) and marginal pdfs for (b) β, (c) α, (d) calcification depth z, and (e) calibration error standard deviation σ.

tails of its distribution than the sample value of this statistic [*DeGroot and Schervish*, 2002], are all quite large, no less than 30%. Therefore the null hypothesis is accepted for the analysis of all species: Model fit is generally consistent with its assumptions. This is not surprising because the model error σ is one of the estimated model parameters.

[24] To inspect model residuals in greater detail, we present scatterplots of measured versus predicted $\delta^{18}O_c$ in Figure 5. Predictions were computed using equation (15). Their estimated theoretical errors (two standard deviations, shown in Figure 5 by horizontal lines) vary strongly between species and sometimes even between cores for

Table 3. Posterior Estimates for Parameters Obtained From Bayesian Analysis[a]

	α, °C		β, °C/‰		z, m		σ, ‰	
Species	Mean	95% Confidence Interval	Mean	95% Confidence Interval	Mean	95% Confidence Interval	Mean	95% Confidence Interval
G. ruber (white)	15.4	14.1–16.8	4.78	4.18–5.26	15.9	0.0–33.6	0.26	0.20–0.33
G. ruber (pink)	14.7	13.4–16.6	4.86	4.12–5.27	21.1	3.1–39.0	0.24	0.18–0.31
G. sacculifer	16.2	15.4–16.9	4.94	4.57–5.26	29.2	18.0–39.6	0.17	0.14–0.23
O. universa	16.5	15.4–17.0	5.11	4.68–5.29	34.9	2.6–61.1	0.50	0.38–0.66
P. obliquiloculata	16.8	16.5–17.0	5.22	5.06–5.30	50.0	40.6–61.9	0.28	0.21–0.39
G. menardii	16.6	16.0–17.0	5.20	5.00–5.30	75.6	63.1–87.3	0.33	0.26–0.43
N. dutertrei	14.6	12.5–16.9	5.09	4.55–5.29	104.0	64.0–169.0	0.49	0.37–0.66
N. tumida	13.1	12.5–14.1	4.95	4.31–5.28	225.5	175.6–273.0	0.33	0.25–0.43

[a]Expected values (means of the posterior probability distribution) and 95% confidence intervals are presented for the calibration intercept α, slope β, calcification depth z, and the standard deviation σ of calibration error.

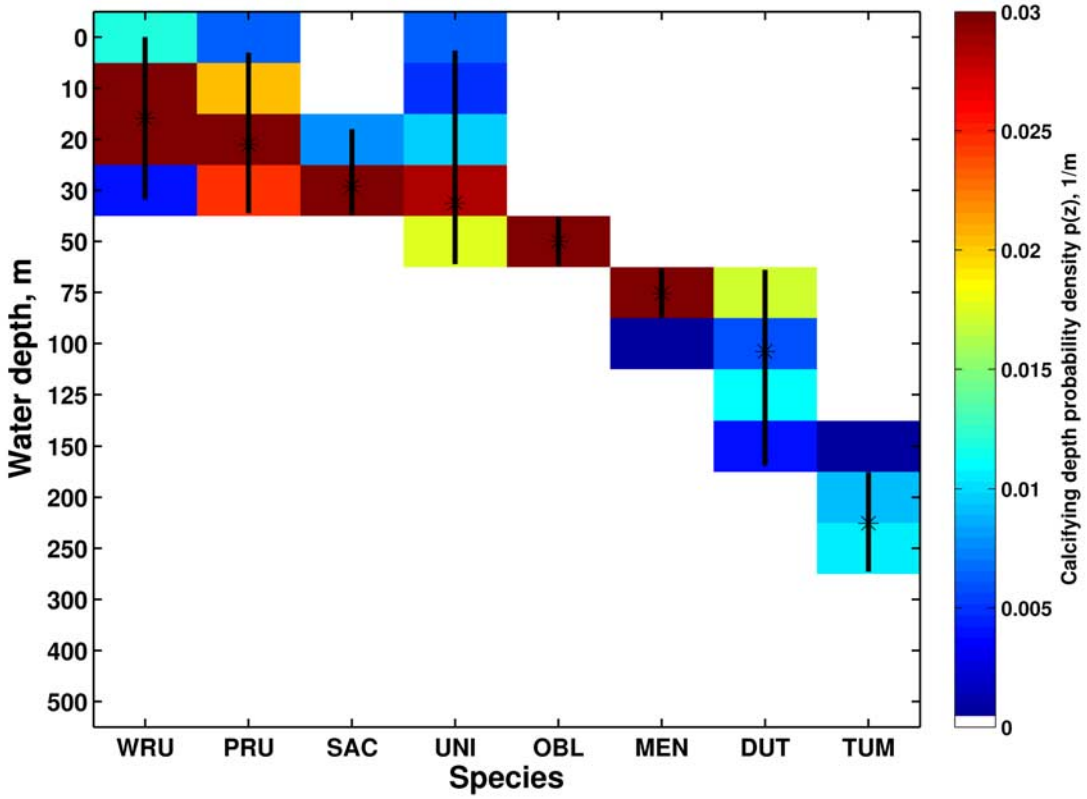

Figure 4. Probability denisity functions for the calcification depth. Color scale saturates at 0.03 m^{-1}. Stars indicate expected values (posterior distribution means). Vertical black lines show 95% confidence intervals. Positions on the horizontal axis correspond to different species: WRU, *G. ruber* (white); PRU, *G. ruber* (pink); SAC, *G. sacculifer* (without final chamber); UNI, *O. universa*; OBL, *P. obliquiloculata*; MEN, *G. menardii*; DUT, *N. dutertrei*; and TUM, *N. tumida*.

individual species. The largest Bayesian prediction errors are for *N. dutertrei* and *O. universa* because the analyses of these species produced larger posterior uncertainty in their calcification depth, particularly in the depth intervals with large temperature variability. Large theoretical prediction errors for $\delta^{18}O_c$ of *G. ruber* (white) and *G. sacculifer*, which stand out visually in Figures 5a and 5c, are expected for the core VM019-284, the location in which large vertical temperature gradients occur, according to the WOA2001 data set. (*G. ruber* (pink) $\delta^{18}O_c$ measurement is not available for this core; thus a point with the large uncertainty is missing in Figure 5b.)

[25] An important characteristic of prediction is its bias. Do we have evidence of prediction bias in the scatterplots of Figure 5? Mean error (ME) of the prediction is a sample mean of the actual differences between measured and predicted $\delta^{18}O_c$. To evaluate their significance, they need to be compared to the error standard deviations (STDE), also estimated from the sample. These parameters are reported in Figures 5a–5g and Table 4. Under normality assumption the null hypothesis that the errors have zero

Table 4. Consistency Tests for Bayesian Analysis and Predictions[a]

		Omnibus χ^2 Test		Student's t Test for the Prediction Bias				Student's t Test for the Prediction Slope			
Species	N	χ^2	p Value	ME, ‰	STDE, ‰	t	p Value	r	σ_r	t	p Value
G. ruber (white)	31	29.9	0.64	0.002	0.26	0.05	0.96	0.97	0.30	−0.1	0.91
G. ruber (pink)	28	26.8	0.63	0.000	0.24	0.01	0.99	0.47	0.27	−2.0	0.06
G. sacculifer	31	30.1	0.62	0.003	0.17	0.09	0.93	1.00	0.19	0.0	0.99
O. universa	27	25.8	0.62	0.089	0.49	0.95	0.35	−0.02	0.44	−2.3	0.03
P. obliquiloculata	24	24.3	0.46	0.109	0.27	1.99	0.06	0.34	0.13	−5.0	0.00
G. menardii	30	29.8	0.55	0.045	0.33	0.75	0.46	0.50	0.08	−6.1	0.00
N. dutertrei	26	28.8	0.30	−0.040	0.46	−0.45	0.66	0.24	0.13	−6.1	0.00
N. tumida	31	30.0	0.63	−0.029	0.32	−0.49	0.63	0.77	0.17	−1.3	0.20

[a]See text for explanations. ME is mean error; STDE is standard deviation.

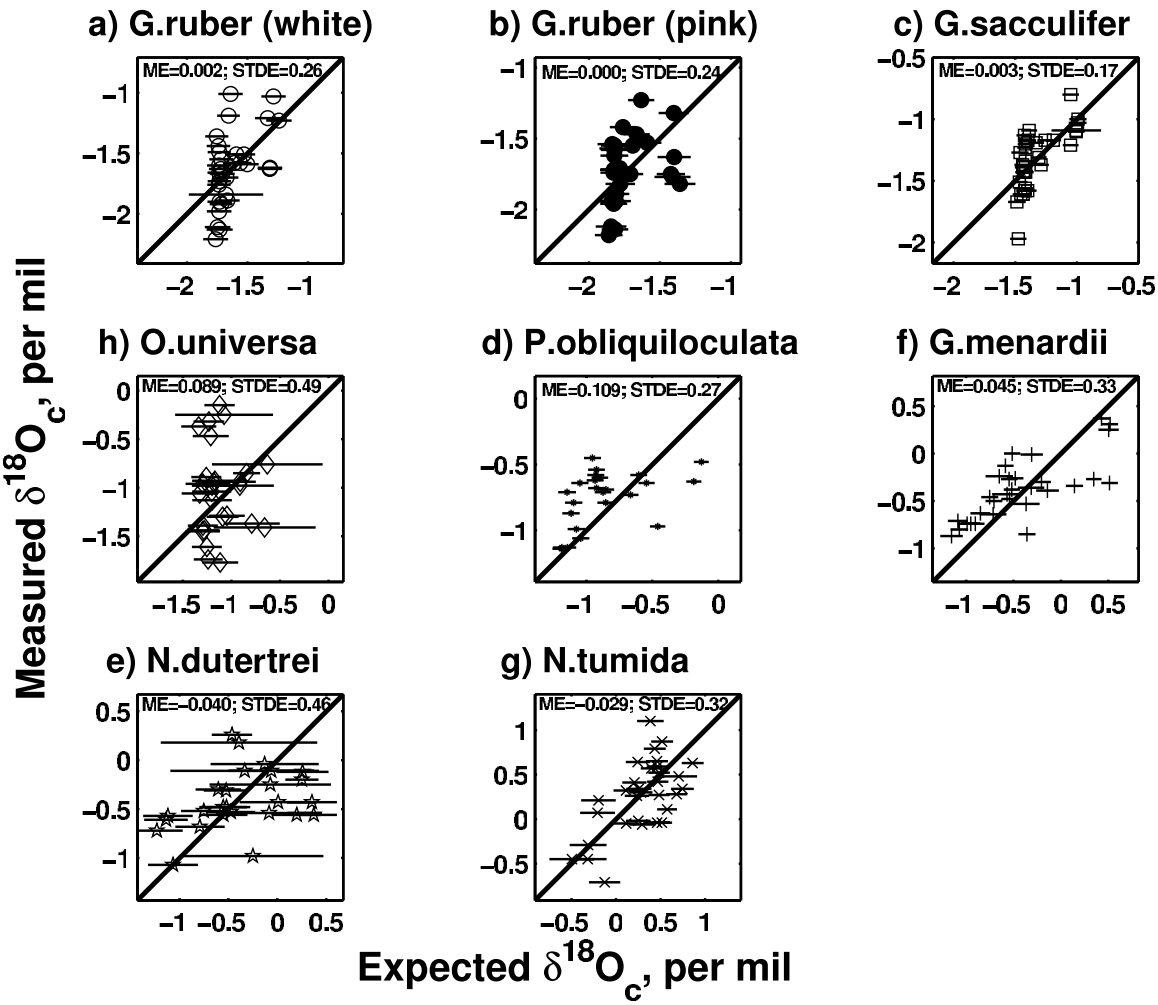

Figure 5. Measured versus predicted (i.e., expected) $\delta^{18}O_c$. Predictions are made using equation (15). Horizontal lines drawn through individual markers show two standard deviations of Bayesian prediction error. Sample mean error (ME) and standard deviation (STDE) of the actual measured − predicted $\delta^{18}O_c$ errors are indicated in Figures 5a–5g.

mean can be tested using Student's t statistics [*DeGroot and Schervish*, 2002]: $t = \sqrt{N} \times \mathrm{ME/STDE}$. Corresponding p values (Table 4) are large for all species except *P. obliquiloculata*, but even for them the p value is 0.06. Therefore the null hypothesis of unbiased prediction for each species successfully passes the t test with 5% significance.

[26] Lack of bias having been established, one can ask if the predictions in Figure 5 are optimal in terms of the slope of a predictive line. Could we improve the skill by rescaling the predictions up or down? A formal way to address this question is to assume that measurements (M) can be presented as scaled predictions (P) with some offset (C) and random error (ε):

$$M = r \times P + C + \varepsilon. \tag{18}$$

For predictions shown in Figure 5 we effectively use $r = 1$ and $C = 0$. To check if $r = 1$ is consistent with the data, we test the null hypothesis of r being equal to 1 in equation (18) against its two-sided alternative. This is effectively a t test for the slope of a univariate linear regression. If the null hypothesis is true, the test statistic

$$t = (r - 1)/\sigma_r,$$

where r and σ_r are sample regression coefficient and its standard error estimate, respectively, is distributed as Student's t with $N - 2$ degrees of freedom [*DeGroot and Schervish*, 2002, section 10.3, equation (10.3.20)]. Results presented in Table 4 show that the null hypothesis of $r = 1$ passes the test with 5% significance for both variants of *G. ruber*, *G. sacculifer*, and *N. tumida*, but it has to be rejected for the four other species. By equation (7) the slope

of the measured-to-predicted $\delta^{18}O_c$ relationship is, to a large degree, controlled by the model parameter β. Failure of the model, at least for some species, to select parameters that fit data best are discussed in section 4 along with other model limitations.

4. Discussion

4.1. Intercomparison of Calibration Relationships

[27] The model (7) used here can be viewed as a constrained linear regression with some additional parametric dependence of predictors on z. The constraint on the regression coefficients came in a form of the uniform prior distribution for α and β defined by (11). Figure 6a shows a box corresponding to our prior distribution on the (α, β) plane and indicates parameter positions for published calibration equations (1)–(5) (which informed our prior constraints) together with the means of posterior distributions that were obtained in our analyses of different species. All solutions are concentrated in the part of the prior domain corresponding to larger values of β. The 95% confidence intervals for our parameter estimates for most species are quite wide, so they generally cover a large part of the prior domain. Nevertheless, we note that the solution for *N. tumida* is especially close to the relationship obtained by *Bemis et al.* [1998] from culture experiments with 12-chambered *G. bulloides*, while solutions for both variants of *G. ruber* are closest to the calibration from culture experiments with *O. universa* under high-light conditions [*Bemis et al.*, 1998]. Our solution for *O. universa* has within its 95% confidence area the parameters of the *Bemis et al.* [1998] calibration for *O. universa* under low-light conditions, although our solution for *G. sacculifer* is even closer to it.

[28] Figure 6a also demonstrates how prior constraints for β affected solutions for four species: *P. obliquiloculata*, *G. menardii*, *O. universa*, and *N. dutertrei*. Their (α, β) points are particularly close to the highest allowable value in β. Incidentally, these are precisely the species for which the prediction slope was inconsistent with the best fit data (Table 4). In other words, the prior constraint on the allowable range in β prevented the model from selecting higher β values for these species, even though higher values would fit the available data better.

[29] Are larger values of β, implied by these analyses, real or an artefact of relatively small sample sizes (around 30) and perhaps some systematic error? Figure 6b plots calibration lines corresponding to all (α, β) points in Figure 6a together with data points of temperature versus oxygen isotope ratio difference, both evaluated at the species' calcification depths by

$$T_{\mathrm{calc}} = \int T(z)p(z)dz,$$
$$\left[\delta^{18}O_c - \delta^{18}O_w\right]_{\mathrm{calc}} = \delta^{18}O_c - \int \delta^{18}O_w(z)p(z)dz, \quad (19)$$

where $p(z)$ is the species-dependent posterior marginal density function for the calcification depth z. In the context of the general scatter of observational points and the spread of calibration lines (reaching almost 4°C in temperature and 0.8‰ in $\delta^{18}O$), different calibration lines look almost parallel; their slopes appear consistent with the large-scale cross-species arrangement of the data. In fact, a standard unconstrained linear best fit to this entire multispecies data set produces a line (red in Figure 6) with parameters α = 15.3 and β = 5.11, which are within the range of published calibrations. Note that the slope of this line is controlled not by the scatter of points for individual species but by the general shifts of individual species' subsets with regard to each other.

[30] The latter conclusion is consistent with our earlier observation of no significant bias in $\delta^{18}O_c$ predictions for individual species (Table 4). Since mean shifts in measured $\delta^{18}O_c$ and calcification interval temperatures between individual species might be as large as the data point scatter within species, these data sets of individual species, when pooled together, extend along their assumed (and almost parallel) calibration lines. This phenomenon is illustrated further by Figure 7, where the scatterplots of Figures 5a–5g are presented. Even though the STDE in Figure 7 (0.33‰) is in the range of STDE values in Figures 5a–5g (0.17–0.49‰), the normalized prediction skill, which can be measured by the signal-to-noise ratio, is much higher in Figure 7 than in Figures 5a–5g. The reason for this is a larger "signal" variability: The range of measured $\delta^{18}O_c$ exceeds 3‰ in Figure 7, while these ranges are smaller by at least a factor of 2 in most of Figure 5.

[31] A contrast in prediction skill between data sets of individual species in Figure 5 and the multispecies data set in Figure 7 emphasizes better consistency of measured $\delta^{18}O_c$ with typical calibration relationships for "vertical direction," i.e., for different species, which calcify at different depths in the same location, than for "horizontal direction," i.e., for the same species at different geographic locations. Obviously, something hurts the prediction skill for individual species in data sets which include multiple locations.

[32] Figure 7 provides an opportunity for putting our analysis results in the context of that of *Schmidt and Mulitza* [2002, Figure 8, right panel]. Their root-mean-square analysis error is 0.53‰. It was obtained for a global data set, with $\delta^{18}O_c$ varying from −3 to 4‰. Their selection of species also differed from ours: It included three species which we had (*G. ruber*, white and pink variants, and *G. sacculifer*) and three species which we did not use (*N. pachyderma*, left- and right-coiling variants, and *G. bulloides*).

4.2. Caveats of the Analysis

[33] One particular weakness of this data set is the lack of precise age control on the core top sediment samples. Using a foraminiferal sample from an older core top in locations of slower sedimentation rate can bias the results of our comparison with modern temperatures because the sampled foraminifera have grown in systematically different temperature regimes. In an attempt to identify such cores we plot their temperature profiles in Figure 8 along with $\delta^{18}O_c$-based temperature predictions from our analysis. Visual

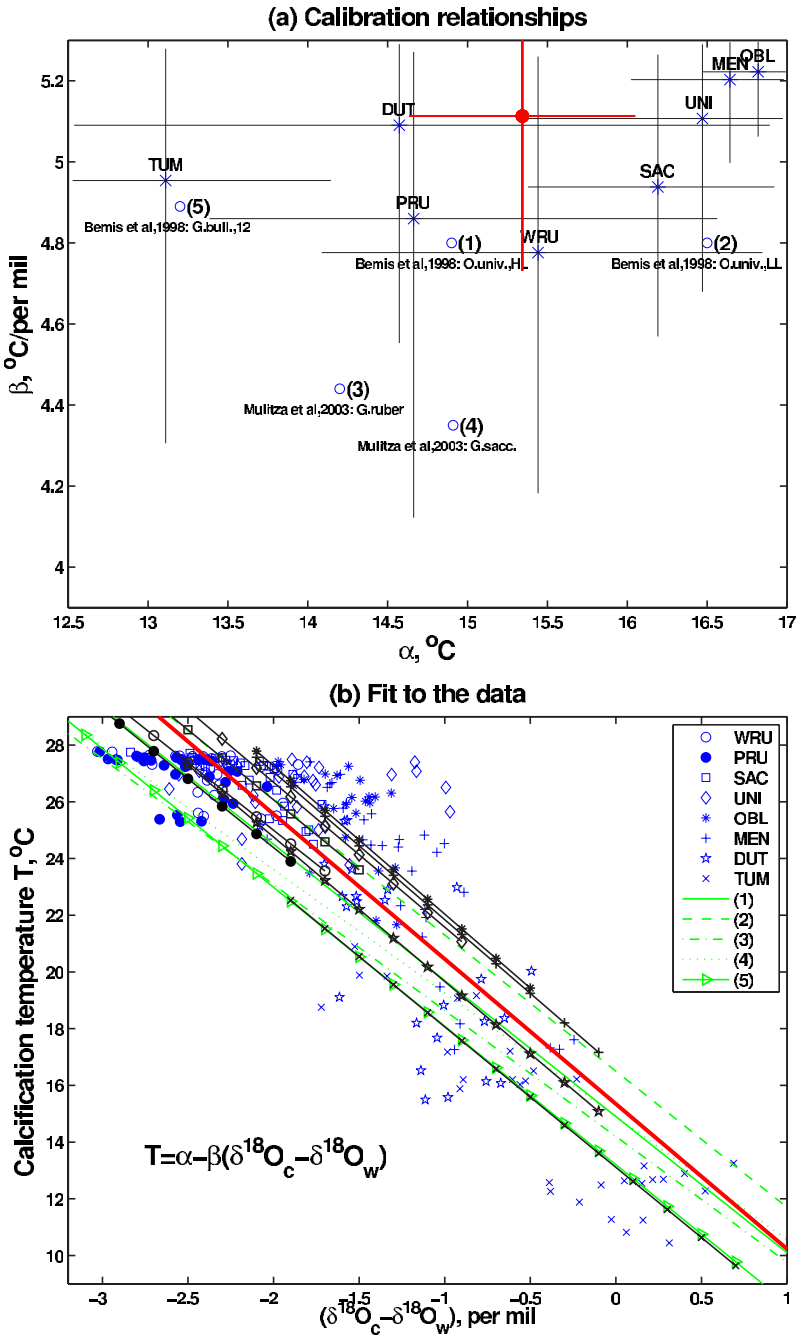

Figure 6. (a) Published and estimated calibration relationships. Open circles mark (α, β) pairs for published calibration equations (1)–(5); crosses indicate posterior means obtained in the present analysis for different species; horizontal and vertical lines drawn through crosses show 95% confidence intervals for α and β, respectively; parameters of the simultaneous linear best fit to all data in Figure 6b and their two standard errors are shown in red. (b) Scatterplot of calcification depth temperatures versus $\delta^{18}O_c$-$\delta^{18}O_w$, estimated by equation (19), shown along with the calibration lines defined by equations (1)–(5) and by (α, β) posterior means from present analyses (identified by species symbols). Red line is the linear best fit to all data in this plot.

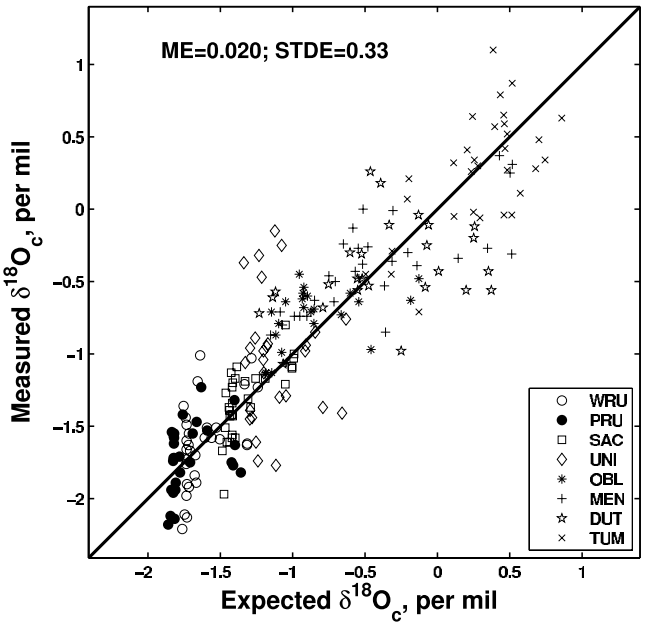

Figure 7. Comparison of measured and predicted $\delta^{18}O_c$ values. Data from Figures 5a–5g are pooled together.

inspection does not identify any cores which are consistently offset. Temperature estimates are generally within 3°C of colocated WOA2001 profiles, most outliers being associated with *O. universa*, *N. dutertrei*, and *N. tumida*, species with large uncertainty in their calcification depth estimates. This conclusion is also confirmed by Figure 6b, which shows some increase in the scatter near ocean surface (at high temperatures). Part of this increase is due to the diminished representativeness of WOA2001 temperatures near the surface, where trends and decadal variability are larger than at depth, but high $\delta^{18}O_c$ and high-temperature *O. universa* outliers contributed to the increase as well.

[34] The *O. universa* example highlights the obvious weakness in our analysis: an assumption that each species calcifies at a single depth. This assumption is known to be wrong for *O. universa* and likely has resulted in large depth uncertainty and the largest prediction error for this species in our analysis. Yet, because of the assumption of a single depth, we might still have underestimated the uncertainty in its depth interval. Relaxing the assumption of a single depth in our analysis, along with the introduction of other controlling parameters (light, density, nutrients, and seasonality) that the species might optimize in choosing their habitat, can improve the model performance and help with better interpretations for species able to live under a variety of environmental conditions.

[35] The possibility that some species form a secondary calcite layer can also be addressed by allowing more than one calcification depth interval in the model at least theoretically. For example, *G. sacculifer* is known to form 20–30% of secondary calcite by weight [*Lohmann*, 1995]. This estimate was reconfirmed in the global analysis by *Schmidt and Mulitza* [2002]. In our analysis, however, considering the narrowness of the calcification depth interval that we obtained for *G. sacculifer* with the present model, it is unlikely that we could reliably derive an additional, much deeper, calcification depth interval for *G. sacculifer* from the small-size data set that we are analyzing here, even if our model were given this flexibility.

[36] Since we allow species-dependent adjustments of calibration coefficients in the model, mean impacts of the "vital" effect (species-specific fractionation due to biophysical processes) over the entire data set can be absorbed by some change in α. Similarly, the mean impact of carbonate ion concentration $[CO_3^{2-}]$ on $\delta^{18}O_c$ [*Zeebe*, 1999; *Schmidt and Mulitza*, 2002] can be compensated for by changes in both α and β. To identify effects like that in an unambiguous way, they not only need to be introduced into the model but will also require a larger core top data set, featuring significant variations of these effects from one location to another.

[37] Annual mean temperature and $\delta^{18}O_w$ values of the modern period used in this work are subject to measurement, sampling, and analysis error: Gridded WOA2001 and *LeGrande and Schmidt* [2006] data sets were produced by interpolation and smoothing of sparse observations. The smoothing may have introduced some false consistency into the gridded data, masking partly its natural variability. The data sets' own errors, however, are most likely dwarfed by the errors introduced in our usage of these data: a lack of control for the species' seasonality or precise time period of the core top sample.

[38] The main remaining problem in the interpretation of this data set is evident in the clustered, and thus possibly nonrandom, deviations from the one-to-one line in Figures 5a–5g. Some effects which change from place to place and from species to species must be at work there, creating these deviations from our estimates of calibration line at calcification depths. What is their nature: age variations, additional controlling factors, nonconstant vital effects, seasonality? The data set in its present form is too small to identify these unknown effects; a larger database could produce a clearer picture. Radiocarbon age control of core top samples as well as the development of species-specific calibration equations are other directions where future progress can help reduce uncertainties in the analyses of this and similar data sets.

5. Conclusions

[39] Measured $\delta^{18}O_c$ of eight species of planktonic foraminifera from 31 tropical Atlantic sediment core tops is consistent with upper ocean temperatures and $\delta^{18}O_w$ at various water depths at the core locations and with ecological water depth preferences of these species known from plankton tow and sediment trap abundance data. Bayesian statistical analysis highlighted this correspondence.

[40] Continuous distribution of apparent calcification depths for these species throughout the top 250 m (Figure 4) suggests that a reconstruction of thermocline profiles based on a multispecies approach may yield higher-resolution thermocline reconstructions than have been possible previously. We envision multiple regression using a matrix inversion approach, in which a multipoint thermocline profile may be reconstructed rather than a simple thermocline depth.

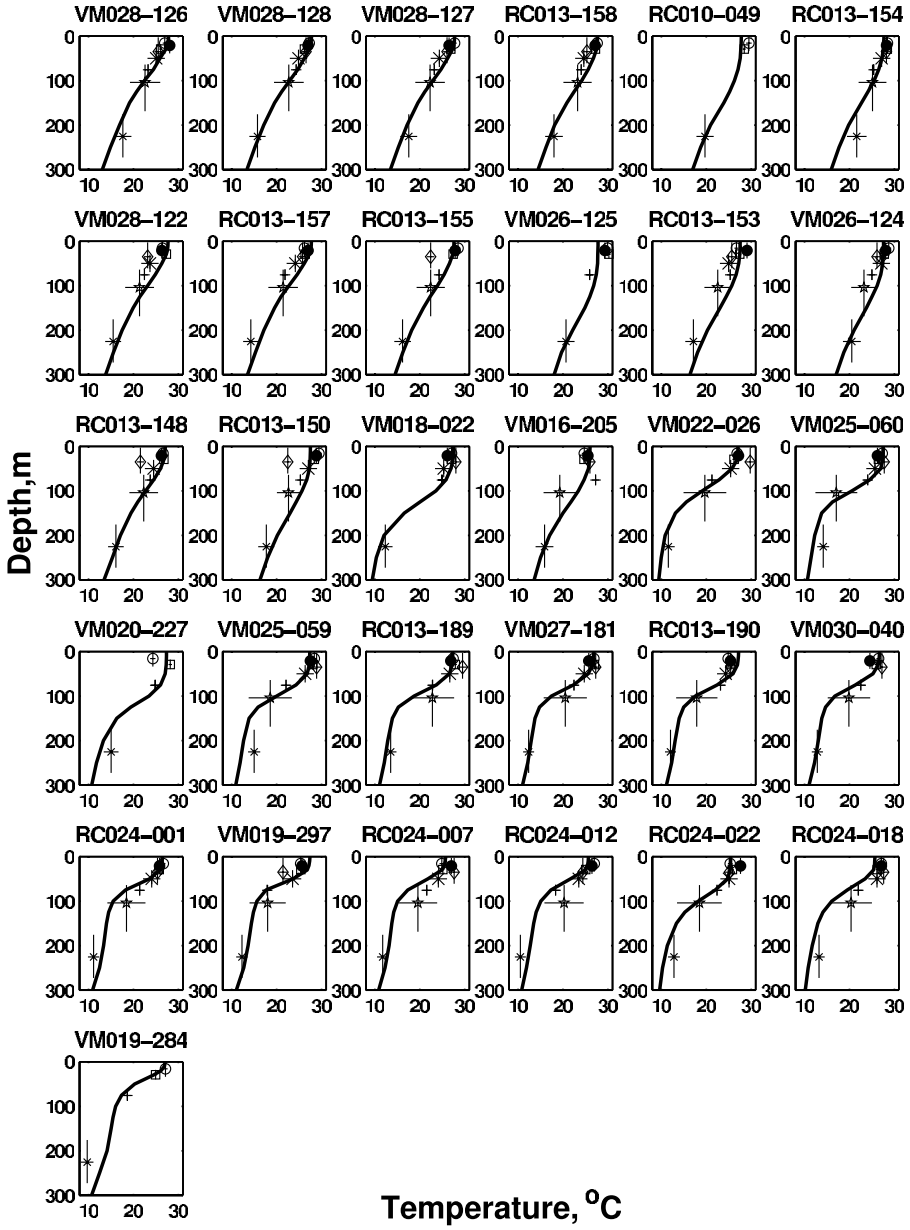

Figure 8. Comparison of observed and predicted by equation (16) temperature values. Markers identify different species according to the legend from Figure 7. Vertical lines through markers are 95% confidence intervals for the calcification depth; horizontal lines are two standard errors for temperature predictions.

[41] Some of the species studied here have not been subject to rigorous attempts to calibrate their $\delta^{18}O_c$ as paleotemperature proxies. New data relating $\delta^{18}O_c$ of deep dwelling species *G. menardii* and *N. tumida* to ocean temperatures at roughly 75 m and 175–275 m, respectively, highlight the potential contributions these species can make to further development of paleotemperature reconstructions.

[42] **Acknowledgments.** This research was supported by grants from the Climate Center of LDEO and a Graduate Research Environmental Fellowship to E.C.F. from the Global Change Education Program, which is administered by the Oak Ridge Institute for Science and Education for the U.S. Department of Energy's Office of Biological and Environmental Research. A.K. was supported by the NSF grants ATM04-17909 and OCE 03-17941. Samples were supplied by the LDEO Deep-Sea Sample Repository, and Martha Dees and Linda Baker provided expert guidance in sample preparation and analysis. Early versions benefited greatly from discussion with Yair Rosenthal, and constructive criticism from two anonymous reviewers greatly improved the manuscript. LDEO contribution 7025.

References

Anand, P., H. Elderfield, and M. H. Conte (2003), Calibration of Mg/Ca thermometry in planktonic foraminifera from a sediment trap time series, *Paleoceanography*, *18*(2), 1050, doi:10.1029/2002PA000846.

Bé, A. W. H., and D. S. Tolderlund (1971), Distribution and ecology of living planktonic foraminifera in surface waters of the Atlantic and Indian oceans, in *Micropaleontology of Oceans*, edited by B. M. Funnell and W. R. Riedel, pp. 105–149, Cambridge Univ. Press, London.

Bemis, B. E., H. J. Spero, J. Bijma, and D. W. Lea (1998), Reevaluation of the oxygen isotopic composition of planktonic foraminifera: Experimental results and revised paleotemperature equations, *Paleoceanography*, *13*(2), 150–160.

Bemis, B. E., H. J. Spero, and R. C. Thunell (2002), Using species-specific paleotemperature equations with foraminifera: A case study in the Southern California Bight, *Mar. Micropaleontol.*, *46*, 405–430.

Berger, W. H. (1981), Oxygen and carbon isotopes in foraminifera - An introduction, *Palaeogeogr. Palaeoclimatol. Palaeoecol.*, *33*(1–3), 3–7.

Broecker, W. S., and T. Takahashi (1978), Relationship between lysocline depth and in situ carbonate ion concentration, *Deep Sea Res.*, *25*(1), 65–95.

Conkright, M. E., R. A. Locarnini, H. E. Garcia, T. D. O'Brien, T. P. Boyer, C. Stephens, and J. I. Antonov (2002), World ocean atlas 2001: Objective analyses, data statistics, and figures, CD-ROM documentation, *NODC Internal Rep. 17*, 17 pp., Natl. Oceanogr. Data Cent., Silver Spring, Md.

Craig, H., and L. I. Gordon (1965), Deuterium and oxygen-18 variations in the ocean and the marine atmosphere, in *Spoleto Conference on Stable Isotopes in Oceanographic Studies and Palaeotemperatures*, edited by E. Tongiorgi, pp. 9–130, Cons. Naz. delle Ric. Lab. di Geol. Nucl., Rome.

DeGroot, M. H., and M. J. Schervish (2002), *Probability and Statistics*, 3rd ed., 816 pp., Addison-Wesley, Boston, Mass.

Dekens, P. S., D. W. Lea, D. K. Pak, and H. J. Spero (2002), Core top calibration of Mg/Ca in tropical foraminifera: Refining paleotemperature estimation, *Geochem. Geophys. Geosyst.*, *3*(4), 1022, doi:10.1029/2001GC000200.

Deuser, W. G., and E. H. Ross (1989), Seasonally abundant planktonic-foraminifera of the Sargasso Sea; succession, deep-water fluxes, isotopic compositions, and paleoceanographic implications, *J. Foraminiferal Res.*, *19*, 268–293.

Fairbanks, N. R. G., and P. H. Wiebe (1980), Foraminifera and chlorophyll maximum: Vertical distribution, seasonal succession, and paleoceanographic significance, *Science*, *209*, 1524–1526.

Gelman, A., J. B. Carlin, H. S. Stern, and D. B. Rubin (2004), *Bayesian Data Analysis*, 2nd ed., 668 pp., CRC Press, Boca Raton, Fla.

LeGrande, A. N., and G. A. Schmidt (2006), Global gridded data set of the oxygen isotopic composition in seawater, *Geophys. Res. Lett.*, *33*, L12604, doi:10.1029/2006GL026011.

LeGrande, A. N., J. Lynch-Stieglitz, and E. C. Farmer (2004), Oxygen isotopic composition of *Globorotalia truncatulinoides* as a proxy for intermediate depth density, *Paleoceanography*, *19*, PA4025, doi:10.1029/2004PA001045.

Lohmann, G. P. (1995), A model for variation in the chemistry of planktonic-foraminifera due to secondary calcification and selective dissolution, *Paleoceanography*, *10*(3), 445–457.

Mulitza, S., A. Dürkoop, W. Hale, G. Wefer, and H. S. Niebler (1997), Planktonic foraminifera as recorders of past surface-water stratification, *Geology*, *25*, 335–338.

Mulitza, S., T. Wolff, J. Patzold, W. Hale, and G. Wefer (1998), Temperature sensitivity of planktonic foraminifera and its influence on the oxygen isotope record, *Mar. Micropaleontol.*, *33*, 223–240.

Mulitza, S., D. Boltovskoy, B. Donner, H. Meggers, A. Paul, and G. Wefer (2003), Temperature: $\delta^{18}O$ relationships of planktonic foraminifera collected from surface waters, *Palaeogeogr. Palaeoclimatol. Palaeoecol.*, *202*(1–2), 143–152.

Ravelo, A. C., and N. R. G. Fairbanks (1992), Oxygen isotopic composition of multiple species of planktonic foraminifera: Recorders of the modern photic zone temperature gradient, *Paleoceanography*, *7*(6), 815–831.

Sarmiento, J. L., N. Gruber, M. A. Brzezinski, and J. P. Dunne (2004), High-latitude controls of thermocline nutrients and low latitude biological productivity, *Nature*, *427*, 56–60.

Schmidt, G. A. (1999), Forward modeling of carbonate proxy data from planktonic foraminifera using oxygen isotope tracers in a global ocean model, *Paleoceanography*, *14*(4), 482–497.

Schmidt, G. A., and S. Mulitza (2002), Global calibration of ecological models for planktic foraminifera from coretop carbonate oxygen-18, *Mar. Micropaleontol.*, *44*, 125–140.

Zeebe, R. E. (1999), An explanation of the effect of seawater carbonate concentration on foraminiferal oxygen isotopes, *Geochim. Cosmochim. Acta*, *63*, 2001–2007.

P. B. de Menocal and A. Kaplan, Lamont-Doherty Earth Observatory of Columbia University, Palisades, NY 10964, USA.

E. C. Farmer, Geology Department, Hofstra University, 145 Gittleson, Hempstead, NY 11549-1140, USA. (geoecf@hofstra.edu)

J. Lynch-Stieglitz, School of Earth and Atmospheric Sciences, Georgia Institute of Technology, 311 Ferst Drive, Atlanta, GA 30332, USA.